Publisher's version: 5. Jamshidi, R., Lake, C.B., and Barnes, C. 2015. Evaluating impact resonance testing as a tool for predicting hydraulic conductivity and strength changes in cement-stabilized soils, ASCE Journal of Materials in Civil Engineering, 27(12): 04015051-1- 04015051-9, 10.1061/(ASCE)MT.1943-5533.0001318, 04015051.

Evaluating Impact Resonance Testing as a Tool for Predicting Hydraulic Conductivity and Strength Changes in Cement-Stabilized Soils

Reza Jolous Jamshidi[1], Craig B. Lake[2]*, and Christopher L. Barnes[3]

[1]Ph.D. Candidate, Civil and Resource Engineering Department, Dalhousie University, Canada.

[2]Associate Professor and Head, Civil and Resource Engineering Department, Dalhousie University, Canada.

[3]Senior Materials Engineer, AMEC Environment and Infrastructure, Dartmouth, Nova Scotia, Canada; and, Adjunct Professor, Civil and Resource Engineering Department, Dalhousie University, Canada.

*Corresponding author. E-mail: craig.lake@dal.ca, Tel.: +1 (902) 494 3220.

Abstract

In this paper the impact resonance (IR) test method is used as a non-destructive tool to examine the curing progression, freeze/thaw (f/t) resistance, and healing potential of cement-stabilized soils. Resonant frequency (RF) measurements on specimens moist-cured for up to 241 days indicate that the main portion of the hydration process is completed after about 60 days. Results of RF measurements on immature (i.e. cured for 16 days) and mature (i.e. cured for over 110 days) specimens exposed to 12 cycles of f/t indicate that the initial f/t exposure had a significant effect on the degradation of the structure. After the initial f/t cycle, some specimens exhibited continued reductions in RF values to as low as 10 percent of the initial measurements, while several specimens showed signs of recovery leading to minor increases in the RF values. Changes in RF values are compared to the hydraulic conductivity changes measured on the same specimens reported in a previous publication by the authors. Based on the results, a pre-screening scheme is proposed that can significantly reduce the time required for f/t studies of cement-stabilized soils. Also, RF measurements after 120 days of a post-exposure healing period show a significant potential for recovery in RF values for f/t exposed specimens. However, the recoveries in RF values are not proportional to the hydraulic conductivity recovery of the specimens.

Keywords:

Freeze, Thaw, Soil, Cement, Resonant Frequency, Hydraulic Conductivity, Impact Resonance.

INTRODUCTION

Cement-treatment of soils is an established method for improving their strength and hydraulic performance (ACI 1990; ACI 1999). Previous studies (e.g. Klich et al. 1999; Fitch & Cheeseman 2003) showed that despite improved mechanical properties after treatment, cement-treated materials can undergo degradation under environmental exposure such as freezing/thawing (f/t) cycles. Currently there is no standard method for assessing the hydraulic performance of cement-stabilized materials in cold regions. Durability studies for cement-treated materials intended for applications requiring low hydraulic conductivity values, such as cement-based solidification/stabilization, have suggested percent mass loss as an indicator of acceptability for performance under f/t exposure (e.g. Stegemann & Côté 1996; Paria & Yuet 2006; ITRC 2011). While percent mass loss may sufficiently correlate with the changes in strength related parameters (e.g. Shihata & Baghdadi 2001), Jamshidi & Lake (2014) showed that it is not a reliable indicator for predicting changes in the hydraulic conductivity of cement-stabilized soils exposed to f/t cycles. Further, conducting performance monitoring experiments, such as hydraulic conductivity measurement, prior to and after f/t exposure can add a significant amount of time to an already laborious testing process of these materials. Hence, development of quick predictive tools for assessment of hydraulic conductivity changes in cement-stabilized soils during freezing exposure would appear to be beneficial.

Vibration-based, non-destructive techniques are commonly used to evaluate the dynamic properties of structures incorporating different materials in civil engineering applications. These techniques have been used in evaluation of cement-based materials, mainly concrete, to predict dynamic modulus of elasticity (Swamy & Rigby 1971; ASTM-C215 2008), monitor changes due to progression of the hydration process (Nagy 1997; Jin & Li 2001), or track damage formation during cyclic loads (Shah et al. 2000; Gheorghiu et al. 2005) and f/t exposure (El-Korchi et al. 1989; Ababneh & Xi 2006; ASTM-C666 2008). These techniques rely on the principle that the resonant frequency (RF) of a structure is related to its physical properties including density, shape, and the dynamic modulus of elasticity (Malhotra 2011). Any changes in the physical properties of a structure will subsequently alter the measured RF of the system. Therefore, vibration-based, non-destructive techniques are potentially efficient tools for monitoring degradation or improvement (e.g. curing processes) in cement-based materials.

Preliminary work by Jamshidi et al. (2014) showed that the variations in the RF values measured using the impact resonance (IR) method during different f/t exposure scenarios was consistent with the observed changes in the hydraulic conductivity and unconfined compressive strength (UCS) of a cement-stabilized silty sand. The purpose of the current study was to further assess the suitability of the IR technique in replacing or supplementing the current industrial practice for evaluating the f/t performance of cement-stabilized soils. To achieve this objective, the IR method was used to monitor changes in the structure of several cement-treated soils due to cement hydration (i.e. curing), f/t damage, and post f/t exposure healing processes. The results of the IR tests from the latter two experiments were compared to the hydraulic conductivity changes measured on the same specimens, presented in a previous publication by Jamshidi & Lake (2014). Based on the results a potential pre-screening system is proposed for assessing damage (i.e. changes in the hydraulic performance) in cement-stabilized soils under exposure to f/t cycles.

EXPERIMENTAL PROGRAM

The IR method testing conditions and experimental program are discussed in the current section. The majority of the IR experiments presented herein were performed on specimens in a previous study by Jamshidi & Lake 2014. A comprehensive discussion on the materials used, specimen preparation, and f/t testing conditions were presented by Jamshidi & Lake (2014). For the sake of completeness, only a summary of this information is presented herein.

Specimen Preparation

Three different soils (i.e. SI, SII, and SIII) were manufactured by blending "soil A" (size fraction between 0.08 mm and 9.5 mm of a glacially derived silty sand (SM) (ASTM-D2487 (2011))) and "soil B" (size fraction smaller than 0.08 mm of a silt (ML) (ASTM-D2487 (2011)) derived from quarry operations) according to the proportions presented in Table 1. X-ray diffraction tests performed on powdered samples (i.e. <0.044 mm) of soil A and B suggest quartz and feldspars as the main mineralogical components of these materials (Jamshidi (2014)).

After blending, SI, SII, and SIII soils were stabilized by adding ten percent Portland-limestone blended cement (CSA type GUL) at different water/cement (w/c) ratios (i.e. 1, 1.5, and 2) resulting in nine different mix designs as presented in Table 1. The three soil-cement blends used in the study had an optimum water content in the range of 8 to 11% and a maximum dry density ranging from 1976 to 2050 Kg/m^3 (ASTM-D558 2011). Based on a visual assessment of the mix workability at the time of casting, specimens from each mix design were either compacted in standard compaction molds (ASTM-D558 2011), or placed into plastic molds (with a nominal size of 101 mm diameter and 118 mm height) for self-consolidation (see Table 1). For all mix designs, the constituents were mixed using a drill-mounted paddle until uniformity was reached. After the soil-cement mixture was placed in the molds, they were sealed for 5 days in air-tight plastic bags to minimize water evaporation prior to extrusion. Specimens were then stored in a humidity-controlled curing room until the required age for the start of each experiment.

Impact Resonance (IR) Test

A detailed procedure for conducting IR tests to measure fundamental transverse, longitudinal, and torsional RF of concrete specimens can be found in ASTM-C215 (2008). The set-up used in the current study is presented in Fig. 1. The impact load was generated using a 9.5 mm in diameter steel ball attached to a plastic band, with a combined mass of 5.3 g and was applied to the axial centerline of the specimens. An accelerometer (PCB model 352C68) was magnetically connected to a small piece of steel glued on the opposite side of the specimen. The accelerometer captured the vibration response of the specimen due to the impact and transferred the signals to an amplifier and a computer data acquisition system (Freedom Data PC Platform, Olson Instruments Inc.) for recording and signal processing. A sampling rate of 500 kHz and record size of 8192 samples was used to provide a frequency resolution of 61 Hz for each test. A bandpass filter of 500 to 15000 Hz was applied during the test to isolate frequency components within the expected range of resonances. A fast Fourier transformation (FFT) was then used to transfer the signal to the frequency domain to determine the longitudinal RF of each specimen as the peak spectral amplitude within the response. Each test consisted of five replicate trials on the specimen and the average of the RF values were calculated for comparison in the results section. An average Relative Standard Deviation (RSD) value of less than 1 percent, with a range of 0 to 16.6 percent was calculated based on the five RF measurement trials on each specimen.

Testing Program

Monitoring the Curing Progress

Given that the hydration of cement becomes a slow diffusion-controlled reaction during its initial stages (Mindess et al. 2003), the structure of cement paste continues to change over time as the material moves towards being completely cured. Reductions in the hydraulic conductivity and increases in the strength are expected as a result of the curing progress in cement-based materials (e.g. Powers et al. 1954; ACI 1990). Understanding the rate of changes and the time span over which curing process occurs can be beneficial for implementation of cement-treatment projects in cold regions, as specimens cured for only 16 days have shown slightly better performance under f/t exposure compared to specimens exposed at longer curing times (i.e. over 110 days) (Jamshidi & Lake 2014). This may be due to the ductile behavior of specimens at early curing ages and/or the possible counteractive effect of the curing process with the development of f/t deterioration.

In this research, the curing progress of four different mix designs (i.e. SI(1), SI(2), SIII(1), and SIII(2)) was monitored using the IR method. Longitudinal RF measurements were performed on duplicate specimens at different specimen ages ranging from 5 days when they were de-molded, to 241 days after the specimens were prepared. During this period, specimens were kept in a humidity-controlled curing room in order to provide optimal curing conditions required for the hydration process. UCS tests were performed on duplicate specimens at curing times of 16 and 241 days for each mix design to evaluate the possible relationship between changes in the RF and strength development in the specimens.

Monitoring the Degradation of Specimens Due to F/T Exposure

According to Powers' theory of hydraulic pressure (Powers 1945), when water in the capillary pores of cement paste freezes, ice formation results in the water expanding 9% from its initial volume. In near-saturated conditions, this process results in the development of excess pore water pressures in the structure that forces the water to escape to the nearest unsaturated voids/spaces. If the magnitude of the hydraulic pressure developed during this process exceeds the bursting strength of the material, it can result in development of cracks/micro-cracks within the structure (Powers 1945; Chatterji 2003). Flaws which form during the freezing process can lead to an increase in the hydraulic conductivity, a reduction in the modulus of elasticity, and subsequently decrease in the RF of the material.

Specimens from different mix designs presented in Table 1 were exposed to 12 f/t cycles at immature and mature curing conditions. In the current paper, immature and mature exposed specimens are simply referred as immature and mature specimens. For immature specimens, the initial f/t cycle occurred 16 days after specimen preparation; for mature specimens, f/t cycling began after over 110 days of curing had occurred. It was assumed that after this age, changes in the soil-cement structure due to the curing process were negligible. For each f/t cycle, specimens were initially kept in a freezer at -10±1^{o}C for approximately 24 hours, after which they were transferred to a humidity-controlled curing room and were kept at a temperature of 22±1^{o}C for thawing for approximately 24 hours.

The IR testing was performed on each specimen prior to the initial f/t cycle (control conditions) and at the end of the thawing phase at different intervals through the f/t exposure.

The normalized changes in the longitudinal RF at the mth f/t cycle (β_m), was calculated based on the following equation:

$$\beta_m = \frac{RF_m}{RF_0} \qquad \text{Equation 1}$$

where RF_m and RF_0 are longitudinal resonant frequency values at the end of the mth f/t cycle, and at control conditions (i.e. unexposed), respectively.

Results of RF changes in this experimental study are compared to hydraulic conductivity measurements on the same specimens presented in Jamshidi & Lake (2014).

Recovery Potential for Exposed Specimens

Autogenous (self) healing in concrete structures was reported by Abrams (1913) over a century ago. Different mechanisms including the hydration of unreacted cement, swelling of C-S-H gel, blocking of flow paths by impurities, and crystallization of calcium carbonate may lead to autogenous healing, however the latter is believed to be the mechanism most responsible (Edvardsen 1999). This healing process is believed to be more effective for crack widths smaller than 50 μm, while widths as high as 150 μm have been reported to exhibit partial recovery (Yang et al. 2009).

To evaluate the healing potential under various exposure and mix design scenarios, specimens tested in the previous sub-section were kept in a moist room for a period of at least 120 days after the 12th f/t cycle. IR testing was then performed on the specimens and RF values (i.e. RF_{healed}) were compared to the previous measurements on each specimen. All the measurements were normalized with respect to RF values measured for control conditions (i.e. β_{healed}). Results of the hydraulic conductivity measurements on selected specimens before and after the post-exposure healing period presented in Jamshidi & Lake (2014) are also compared to the recovery potential for RF values in the current study.

RESULTS AND DISCUSSIONS

Results of the current study are discussed in the following three sub-sections. First, the curing progression in specimens from selected mix designs is evaluated by presenting the changes in the RF and UCS values over time. Then, damage development in specimens exposed to f/t cycles is discussed using the results from IR tests. Results from this sub-section are compared to hydraulic conductivity changes measured on the same specimens previously presented in Jamshidi & Lake (2014). Finally, the recovery potential for specimens from different mix designs are evaluated using the IR method for f/t damaged specimens after a period of post-exposure curing in a humidity-controlled room.

Assessment of the Curing Progress

Duplicate specimens from four mix designs (i.e. SI(1), SI(2), SIII(1), and SIII(2)) were tested for RF values at different time intervals ranging from 5 to 241 days after casting. Specimens were cured in a humidity-controlled curing room during this period. Average RF values for each mix design are plotted in Fig. 2. Immediately after de-molding, RF values ranged from 6700 to 11600 Hz for the different mix designs. Values increased sharply until a curing age of nearly 60 days, after which they reached about 80 percent of the total observed increase. After this age, the changes in the RF values continued, but at a reduced rate.

Table 2 presents the average RF and UCS values for specimens cured for 16 and 241 days. UCS values ranged from 2.8 to 10.9 MPa for specimens cured for 16 days and from 4.1 to 14.1 MPa for specimens cured for 241 days, showing between a 23 to 52 percent increase in the values (i.e. UCS_{241}/UCS_{16} of 1.23 to 1.52). Comparing the RF between day 16 and 241 shows 11 to 25 percent increase (i.e. RF_{241}/RF_{16} of 1.11 to 1.25). Table 2 shows that within each soil type, specimens with higher RF ratios (RF_{241}/RF_{16}) exhibit higher increases in the UCS values (i.e. higher UCS ratio).

Comparing the results for each soil in Table 2 also shows that mix designs having a lower w/c ratio (i.e. SI(1) and SIII(1)) exhibit higher RF and UCS values. Further, these specimens exhibit smaller increases in RF and UCS values at the longer curing times, which may be due to the unavailability of sufficient amount of water for complete hydration in these specimens.

Relative Standard Deviation (RSD) values for measurements in Table 2 show a maximum of 1.7 and 12.4 percent for IR and UCS tests, respectively. Small RSD values for RF measurements indicate strong reproducibility of results from IR test.

Damage Progression Due to F/T Exposure

RF measurements were performed on duplicate specimens from different mix designs presented in Table 1 prior to f/t exposure (i.e. control conditions) and at subsequently increasing f/t cycles. Fig. 3 shows the typical normalized acceleration responses of a specimen (i.e. SI(1.5)-mature) which was damaged through consecutive f/t cycles. It should be noted that damage is defined as an increase in the hydraulic conductivity value after f/t cycling. It can be seen that the damping (i.e. reduction in the amplitude of the acceleration response after each oscillation) dramatically increases after f/t exposure, resulting in fewer oscillations in signals from cycle 1 and 12 compared to the healthy signal obtained for control conditions. Applying a fast Fourier transformation (FFT) on the signals in Fig. 3, one can plot the frequency spectrum of the SI(1.5)-mature specimen at different f/t exposure levels as presented in Fig. 4. Results show a decrease in RF value as a result of damage progression in the specimen; dropping from about 11700 Hz for control conditions to less than 3000 Hz at the end of the 12th cycle. Alterations observed in the acceleration-time domains and the corresponding frequency patterns are a result of the development of cracks/micro-cracks within the specimen. In the damaged specimens, the impact-generated stress waves reflect from cracks/micro-cracks (formed during f/t cycling) and are forced to travel around them, resulting in energy loss (i.e. increased damping) and reduction in the observed frequencies (Sansalone 1997).

Changes in the RF ratios at different f/t cycles (β_m) are presented in Fig. 5. Results of RF ratios at the end of the 12th f/t cycle (β_{12}) show reductions as high as 90 percent and increases as high as

12 percent in the values. There is no clear trend in the changes of RF ratios (i.e. β_{12}) with respect to the variations in the mix design and soil type. However, within each mix design, mature specimens generally exhibit lower RF ratios (i.e. β_{12}) as compared to immature specimens, indicating a higher degree of structural degradation for mature specimens. This is in agreement with observations reported by Jamshidi & Lake (2014) for hydraulic conductivity changes of immature and mature specimens, which showed higher increases in the hydraulic conductivity values for mature specimens after exposure to f/t cycles.

Immature specimens from some mix designs in Fig. 5 (e.g. SI(1)-immature, SIII(1.5)-immature, and SIII(2)-immature), exhibited some increase in the RF values after exposure to 12 f/t cycles (i.e. $\beta_{12}>1$) compared to values obtained for control conditions (i.e. β_0). This is likely due to the counteractive interference of the hydration process in these specimens, given that f/t exposure occurred at an early curing age, compared to the deteriorating effect of f/t damage. The same specimens exhibited hydraulic conductivity ratios ranging from 0.3 (decrease) to 2 (minor increase) after 12 f/t cycles.

Results in Fig. 5 show that exposure to the initial f/t cycle has a significant influence on the creation of damage. For most cases, even specimens that exhibit higher RF values at the end of the 12th cycle (i.e. $\beta_{12}>1$) show minor drops in values at the end of the first cycle (β_1). This can be explained by the fact that specimens are in near saturated conditions before the initial f/t exposure due to the permeation process during the hydraulic conductivity tests prior to f/t exposure. Considering Power's theory of hydraulic pressure (Powers 1945), after the initial f/t cycle, the possible cracks/micro-cracks developed in the specimens can create a pressure relief opportunity similar to air entrainment in concrete. Assuming that specimens did not fully re-saturate during the thawing phase in the moist room, cracks/micro-cracks can reduce the travel distance for releasing the excess pore water pressures developed during the subsequent freezing phases. Therefore, less damage can be expected in the following f/t cycles as compared to the initial exposure.

After the initial cycle, varying behaviors were observed for specimens at subsequent f/t exposures as noted in Fig. 5. Those include:

- Some specimens exhibited small changes in the RF values after the initial f/t cycle (β_1), with an increase or minor reduction in the frequency values at further f/t exposure. Immature specimens from SI(1), SII(1), SIII(1.5), and SIII(2) fall into this category.
- Some specimens showed a substantial reduction in the RF values after the initial f/t cycle (β_1), but exposure to subsequent cycles resulted in only minor changes in the RF. Immature specimens from SII(1.5), and mature specimens from SII(1), SII(1.5), SIII(1.5), and SIII(2) are in this category.
- Some specimens exhibited a continuous drop in RF values even after the initial f/t cycle. This includes immature specimens from SI(2), SII(2), and SIII(1), and mature specimens from SI(1.5), SI(2), and SIII(1).

Some of the specimens in Fig. 5 did not follow any of the previously mentioned patterns. For instance, RF measurements for SII(2)-mature shows some reduction between cycle 1 and 4, however, no significant variation was observed at subsequent f/t cycles. Also, mature specimens from SI(1) showed an unusual increase in the RF ratios between cycle 8 and cycle 12. For SI(1.5)-immature, due to the unavailability of equipment, RF values were only measured for control conditions and cycle 12. No trend in RF changes can be concluded from these measurements.

Results of RF ratios at the end of the 12th f/t cycle (β_{12}) are plotted against hydraulic conductivity ratios obtained at the end of the 12th cycle (i.e. K_{12}/K_0) in Fig. 6 (a). As previously noted, measurements were performed on the same specimens for both tests. A distinctive behavior was observed for the RF ratio of approximately 0.85. Most specimens having a RF ratio higher than this value, exhibit minor increases or reductions in the hydraulic conductivity values after 12 f/t cycles (i.e. K_{12}/K_0 values close to or smaller than 1). However, specimens with frequency ratios less than approximately 0.85 appeared to exhibit a higher degree of degradation in terms of hydraulic conductivity changes. Similar behavior was observed for RF ratios at the end of the first f/t cycle (i.e. β_1) as presented in Fig. 6 (b).

As mentioned earlier, one of the drawbacks of current test methods for durability assessment of cement-stabilized soils is the long testing time required for f/t cycling of the specimens. This is in addition to an already long curing process, and the need to conduct performance (e.g. hydraulic conductivity) measurement for these materials. A practical application of findings presented in Fig. 6 (b) is to develop a pre-screening scheme based on RF measurements at the end of the initial f/t cycle (i.e. β_1) to enable the prediction of possible hydraulic conductivity changes (in terms of the magnitude) in specimens after exposure to 12 f/t cycles (i.e. K_{12}/K_0). According to the RF ratios, Fig. 6 (b) has been divided into three zones designated as I, II and III. In zone I, for specimens with RF ratios greater than 0.9 at the end of the first f/t cycle (i.e. $\beta_1>0.9$), one can conclude with a great certainty, that there will be minor changes in the hydraulic conductivity values after 12 f/t cycles. As a result, all the specimens in zone I would "pass" the f/t tests performed under conditions demonstrated earlier in the study, if less than an order of magnitude change in hydraulic conductivity values is desired. In zone III, specimens with RF ratios less than 0.7 at the end of the first f/t cycle (i.e. $\beta_1<0.7$), all the specimens seem to show a significant increase (over one order of magnitude) in the hydraulic conductivity values at the end of the 12th cycle, and hence would fail the f/t study tests. For specimens in zone II, with RF values between 0.7 and 0.9 at the end of the initial f/t cycle (i.e. $0.7<\beta_1<0.9$), IR test results are inconclusive and further testing (i.e. exposure to 12 f/t cycles and measurement of hydraulic conductive changes) would be necessary to evaluate the hydraulic performance of specimens. The proposed pre-screening scheme can eliminate the need for completing the 12 f/t cycling of the specimens in zones I and III in order to predict the acceptability of changes in the hydraulic conductivity values as a result of f/t exposure under the conditions demonstrated in this study.

Recovery Potential after the Post-Exposure Healing Period

After exposure to the 12th f/t cycle, previously tested specimens were kept in a moist room for over 120 days. Fig. 7 shows that all specimens exhibited some improvement in their structure after the post-exposure healing period (i.e. $\beta_{healed} > \beta_{12}$). For most cases of immature specimens, with the exception of SI(1.5) and SII(2), average RF values at the end of the healing period reached or exceeded the values obtained as control measurements prior to f/t damage (i.e. $\beta_{healed} \geq 1$). SI(1.5) and SII(2) specimens also showed a noticeable increase in the RF values after the healing periods resulting in an average β_{healed} value of about 0.6.

Considering the case of mature specimens, it can be assumed that the hydration process of cement is nearly complete at the end of the 12th f/t cycle (at the age of over 134 days). In addition, hydraulic conductivity measurements prior to and after f/t cycling minimizes the potential for presence of unreacted cement in the specimens as a result of water permeation within the pore structures. Interestingly, in Fig. 7, mature specimens still exhibit a considerable amount of healing potential as suggested by increases in the RF ratios after the healing period.

Fig. 7 shows that specimens with similar RF ratios after the 12th f/t cycle (β_{12}) do not necessarily exhibit similar recovery potential after the healing period. SII(1)-mature and SII(1.5)-immature both showed a RF ratio of about 0.8 at the end of the 12th cycle; but after the healing period, the RF ratio (β_{healed}) of SII(1.5)-immature increased to a value of about 1, while the RF ratio of SII(1)-mature showed only a small increase. Also, mature specimens from SIII(1), SIII(1.5), and SIII(2) had a RF ratio (β_{12}) ranging from 0.3 to 0.6 at the end of the 12th cycle, however after the healing period, all these specimens reached an average RF ratio (β_{healed}) of about 0.7.

Jamshidi & Lake (2014) discussed the recovery of hydraulic conductivity values for selected f/t damaged specimens from mix designs in Table 1 after the post-exposure healing period. Results are presented in Table 3 and are compared to the changes in the RF values for the same specimens. Based on the results in Table 3, the healing potential for the hydraulic conductivity and RF values do not seem to be proportional. For most of the specimens tested, increases in the RF values after the healing period are significantly more than the improvements in the hydraulic performance. This is potentially a result of the nature of the IR test which involves applying low stress levels to specimens for measurement of the RF values (Jacobsen & Sellevold (1996)). As a result, it is possible that during the healing process minor improvements in the structure of the damaged specimens can improve the RF values, while the overall hydraulic performance of the specimens remains unchanged. Jacobsen & Sellevold (1996) previously showed only minor increases in UCS values for f/t exposed concrete, despite noticeable recovery of RF values after the healing period.

The recovery ratio, defined as the ratio of RF after the healing process (RF_{healed}) divided by RF measured at the end of the 12th f/t cycle (RF_{12}), was calculated and plotted against the hydraulic conductivity ratios (i.e. K_{12}/K_0) in Fig. 8. There seems to be a scattered trend suggesting that specimens with higher hydraulic conductivity ratios (K_{12}/K_0), which indicates higher amount of damage in their structure, also show a higher potential for healing (in terms of recovery of RF values). This observation is likely due to the presence of more cracks/micro-cracks in the highly damaged specimens, which creates a better potential for RF gain during the healing period. However, it should be noted that the superior recovery potential of highly damaged specimens does not necessarily result in a better final performance of these specimens. Considering the case of immature and mature specimens in Fig. 7, mature specimens have an inferior performance under f/t exposure, compared to immature specimens within each mix design. Despite the higher recovery rate for some of the mature specimens (for instance about five times increase in RF for SI(2)-mature between healed conditions and cycle 12), they still exhibit lower RF ratios at the end of the healing period (β_{healed}) as compared to similar conditions for immature specimens exhibiting less initial damage.

SUMMARY AND CONCLUSIONS

The IR method was used as a non-destructive tool to monitor curing progress, f/t damage, and healing process in soil-cement specimens prepared at different mix designs. Results of the RF measurements using this technique were compared to the strength and hydraulic performance of the same specimens. Results showed that IR can be an effective tool in predicting changes in the performance of cement-treated soils. A summary of the specific conclusions from the experimental studies discussed in the previous sections is as follows:

1. RF changes were monitored for specimens from four different mix designs for curing ages ranging from 5 to 241 days. A rapid increase in RF values was observed in the initial 60 days of curing, after which the changes in the RF continued at a slower rate. Comparing RF and UCS

measurements for specimens cured for 16 and 241 days showed that within each soil type, specimens with higher increases in RF values exhibited higher UCS gains.

2. RF measurements on specimens exposed to 12 cycles of f/t showed that the initial cycle has a significant effect in the degradation of the structure. At the end of the 12^{th} f/t cycle, a wide range of behaviours was observed varying from minor increases to decreases of up to 90 percent in the RF values as compared to control measurements performed before f/t exposure.

3. RF ratios at the end of the first (β_1) and 12^{th} (β_{12}) f/t cycles were compared to the hydraulic conductivity ratio (K_{12}/K_0) measurements on the same specimens. Results show IR may have the potential to be used as a non-destructive tool in predicting changes in the hydraulic conductivity of cement-stabilized soils exposed to f/t cycles. Based on the RF measurements at the end of the first f/t cycle, three zones (I, II and III) were proposed. Specimens in zones I ($\beta_1 > 0.9$) would likely to pass the hydraulic performance requirements after 12 cycles of f/t exposure. Specimens in zone III ($\beta_1 < 0.7$) would likely fail the hydraulic performance requirements and would result in significant increases in the hydraulic conductivity values after 12 f/t cycles. The test on specimens with RF ratios between 0.7 and 0.9 ($0.7 < \beta_1 < 0.9$) in zone II is inconclusive, and further f/t cycling and performance monitoring would be required. Using the proposed scheme can significantly reduce the testing time in f/t studies on cement-stabilized soils intended to be used for applications that requires low hydraulic conductivity over the life span of the material.

4. Increases in the RF values were observed for both immature and mature specimens after a post-exposure healing period. Specimens with higher degree of damage seemed to exhibit a higher potential for RF recovery, which is possibly due to the higher number of cracks in these specimens. Healing potential for RF values was not proportional to the recovery of the hydraulic conductivity values for the specimens tested in this study.

ACKNOWLEDGEMENTS

The funding for this project was provided by NSERC through the NSERC CREATE and Discovery grant programs. The authors would like to thank Mitch Woodworth for assistance in the laboratory.

REFERENCES

Ababneh, A.N. and Xi, Y., 2006. Evaluation of environmental degradation of concrete in cold regions. In *Proceedings of Cold Regions Engineering 2006: Current Practices in Cold Regions Engineering*. Edited by M. Davies & J. E. Zufelt. Orono, ME: American Society of Civil Engineers, pp. 1–10.

Abrams, D.A., 1913. *Test of bond between concrete and steel*, Urbana, IL: Bulletin No. 71, Published by the uinversity of Illinois.

ACI, 1999. *Controlled low-strength materials*, Farmington Hills, MI: Americal Concrete Institute (ACI) Committee 229, ACI229R-99.

ACI, 1990. *Report on soil cement*, Farmington Hills, MI: American Concrete Institute (ACI) Committee 230, ACI230.1R-90.

ASTM-C215, 2008. Standard test method for fundamental transverse, longitudinal, and torsional resonant frequencies of concrete specimens. In *Annual Book of ASTM Standards*. West Conshohocken, PA: ASTM International. doi:10.1520/c0215-08.2.

ASTM-C666, 2008. Standard test method for resistance of concrete to rapid freezing and thawing. In *Annual Book of ASTM Standards*. West Conshohocken, PA: ASTM International. doi:10.1520/c0666.

ASTM-D2487, 2011. Standard practice for classification of soils for engineering purposes (unified soil classification system). In *Annual Book of ASTM Standards*. West Conshohocken, PA: ASTM International. doi:10.1520/d2487-11.

ASTM-D558, 2011. Standard test methods for moisture-density (unit weight) relations of soil-cement. In *Annual Book of ASTM Standards*. West Conshohocken, PA: ASTM International. doi:10.1520/d0558-11.

Chatterji, S., 2003. Freezing of air-entrained cement-based materials and specific actions of air-entraining agents. *Cement and Concrete Composites*, **25**(7):pp.759–765. doi:10.1016/s0958-9465(02)00099-9.

Edvardsen, C., 1999. Water permeability and autogenous healing of cracks in concrete. *ACI Materials Journal*, **96**(4):pp.448–54.

El-Korchi, T., Gress, D., Baldwin, K. and Bishop, P., 1989. Evaluating the freeze-thaw durability of Portland cement-stabilized-solidified heavy metal waste using acoustic measurements. In *Environmental Aspects of Stabilization and Solidification of Hazardous and Radioactive Wastes (STP 1033)*. Edited by P. Côté & M. Gilliam. Philadelphia, PA: ASTM International, pp. 184–191. doi:10.1520/stp22878s.

Fitch, J. and Cheeseman, C.R., 2003. Characterisation of environmentally exposed cement-based stabilised/solidified industrial waste. *Journal of Hazardous Materials*, **101**(3):pp.239–255. doi:10.1016/s0304-3894(03)00174-2.

Gheorghiu, C., Rhazi, J.E. and Labossière, P., 2005. Impact resonance method for fatigue damage detection in reinforced concrete beams with carbon fibre reinforced polymer. *Canadian Journal of Civil Engineering*, **32**(6):pp.1093–1102. doi:10.1139/l05-064.

ITRC, 2011. *Development of performance specifications for solidification/stabilization (technical/regulatory guidance)*, Washington, DC: The Interstate Technology & Regulatory Council, Solidification/Stabilization Team.

Jacobsen, S. and Sellevold, E.J., 1996. Self healing of high strength concrete after deterioration by freeze/thaw. *Cement and Concrete Research*, **26**(I):pp.55–62.

Jamshidi, R.J., 2014. *Evaluation of cement-treated soils subjected to cycles of freezing and thawing*. Ph.D. dissertation, Civil and Resource Engineering Department, Dalhousie University, Halifax, Nova Scotia.

Jamshidi, R.J. and Lake, C.B., 2014. Hydraulic and strength performance of three cement-stabilized soils subjected to cycles of freezing and thawing. *Canadian Geotechnical Journal*:pp.1–33.

Jamshidi, R.J., Lake, C.B. and Barnes, C.L., 2014. Examining freeze/thaw cycling and its impact on the hydraulic performance of a cement-treated silty sand. *ASCE Journal of Cold Regions Engineering*.

Jin, X. and Li, Z., 2001. Dynamic property determination for early-age concrete. *ACI Materials Journal*, **98**(5):pp.365–370.

Klich, I., Batchelor, B., Wilding, L.P. and Drees, L.R., 1999. Mineralogical alterations that affect the durability and metals containment of aged solidified and stabilized wastes. *Cement and Concrete Research*, **29**:pp.1433–1440.

Malhotra, V.M., 2011. Nondestructive tests. In *Significance of Tests and Properties of Concrete and Concrete-Making Materials (STP 169D)*. Edited by J. F. Lamond & J. H. Pielert. West Conshohocken, PA: ASTM International, pp. 314–334.

Mindess, S., Young, J.F. and Darwin, D., 2003. *Concrete;* Second Edi., Upper Saddle River, NJ: Pearson Education, Inc.

Nagy, A., 1997. Determintaion of E-modulus of young concrete with nondestructive method. *ASCE Journal of Materials in Civil Engineering*, **9**(1):pp.15–20. doi:10.1061/(asce)0899-1561(1997)9:1(15).

Paria, S. and Yuet, P., 2006. Solidification/stabilization of organic and inorganic contaminants using Portland cement: a literature review. *Journal of Environmental Reviews*, **14**:pp.217–255. doi:10.1139/a06-004.

Powers, T.C., 1945. A working hypothesis for further studies of frost resistance of concrete. *Bulletin no. 5, Portland Cement Association. Research and Development Laboratories.*, **41**(February):pp.245–272.

Powers, T.C., Copeland, L.E., Hayes, J.C. and Mann, H.M., 1954. Permeability of portland cement paste. *Journal of American Concrete Institute*, **51**:pp.285–298.

Sansalone, M., 1997. Impact-Echo: the complete story. *ACI Structural Journal*, **94**(6):pp.777–786.

Shah, S.P., Popovics, J.S., Subramaniam, K. V. and Aldea, C., 2000. New directions in concrete health monitoring technology. *ASCE Journal of Engineering Mechanics*, **126**(7):pp.754–760.

Shihata, S.A. and Baghdadi, Z.A., 2001. Simplified method to assess freeze-thaw durability of soil cement. *ASCE Journal of Materials in Civil Engineering*, **13**(4):pp.243–247.

Stegemann, J.A. and Côté, P.L., 1996. A proposed protocol for evaluation of solidified wastes. *Science of the Total Environment*, **178**(1996):pp.103–110. doi:10.1016/0048-9697(95)04802-2.

Swamy, N. and Rigby, G., 1971. Dynamic properties of hardened paste , mortar and concrete. *Matériaux et Construction*, **1**(4):pp.13–40.

Yang, Y., Lepech, M.D., Yang, E.-H. and Li, V.C., 2009. Autogenous healing of engineered cementitious composites under wet–dry cycles. *Cement and Concrete Research*, **39**(5):pp.382–390. doi:10.1016/j.cemconres.2009.01.013.

Table 1: Summary of soil particle distributions and w/c ratios used in different mix designs (adapted from Jamshidi & Lake (2014)).

Soil name	Mix designation	Water/cement ratio	Mixing method*	Composition by dry weight, %					Classification of blended soil (ASTM-D2487 (2011))
				Soil A				Soil B	
				9.50-4.75 mm	4.75-1.20 mm	1.20-0.30 mm	0.30-0.08 mm	<0.08 mm	
Soil I (SI)	SI(1)	1	C	13	42	30	15	0	Well graded sand
	SI(1.5)	1.5	S						
	SI(2)	2	S						
Soil II (SII)	SII(1)	1	C	11	36	25	13	15	Silty sand
	SII(1.5)	1.5	C						
	SII(2)	2	S						
Soil III (SIII)	SIII(1)	1	C	9	30	21	10	30	Silty sand
	SIII(1.5)	1.5	C						
	SIII(2)	2	S						

*C: Compaction, S: Self-consolidation

Table 2: Comparison of UCS and resonant frequency values at 16 and 241 days.

Soil type	Mix design	Day 16		Day 241		Frequency ratio (RF_{241}/RF_{16})	UCS ratio (UCS_{241}/UCS_{16})
		RF, Hz (RSD, %)	UCS, MPa (RSD, %)	RF, Hz (RSD, %)	UCS, MPa (RSD, %)		
Soil I	SI(1)	13006 (0.2)	10.9 (0.7)	14435 (0.6)	14.1 (0.5)	1.11	1.30
	SI(2)	9234 (1.7)	2.8 (12.4)	11292 (0.0)	4.1 (7.7)	1.23	1.45
Soil III	SIII(1)	11865 (0.5)	10.0 (3.9)	13520 (0.2)	12.3 (1.5)	1.14	1.23
	SIII(2)	8391 (0.4)	3.2 (1.4)	10437 (0.6)	4.9 (2.2)	1.25	1.52

Table 3: Comparison of the healing potential between RF and hydraulic conductivity of the damaged specimens.

Curing condition	Mix design	Specimen #	After the 12th f/t cycle: Hydraulic conductivity ratio, K_{12}/K_0	After the 12th f/t cycle: RF ratio, β_{12}	After the post-exposure healing period: Hydraulic conductivity ratio, K_{healed}/K_0 (% decrease)	After the post-exposure healing period: RF ratio, β_{healed} (% increase)
Immature	SI(1.5)	1	49.2	0.14	5.5 (89)	0.63 (350)
		2	43.5	0.44	2 (95)	0.56 (27)
	SII(1.5)	1	7.8	0.74	1.7 (78)	0.98 (32)
		2	5.4	0.75	2.3 (57)	1.0 (33)
	SII(2)	1	112.5	0.34	54.2 (52)	0.62 (82)
		2	75.0	0.40	13.5 (82)	0.51 (28)
Mature	SI(1.5)	1	298.5	0.39	129.9 (56)	0.74 (90)
		2	1714.3	0.23	1571.4 (8)	0.70 (204)
	SI(2)	1	5250.0	0.10	1250.0 (76)	0.52 (420)
		2	3818.2	0.11	1682.8 (56)	0.51 (364)

List of Figures:

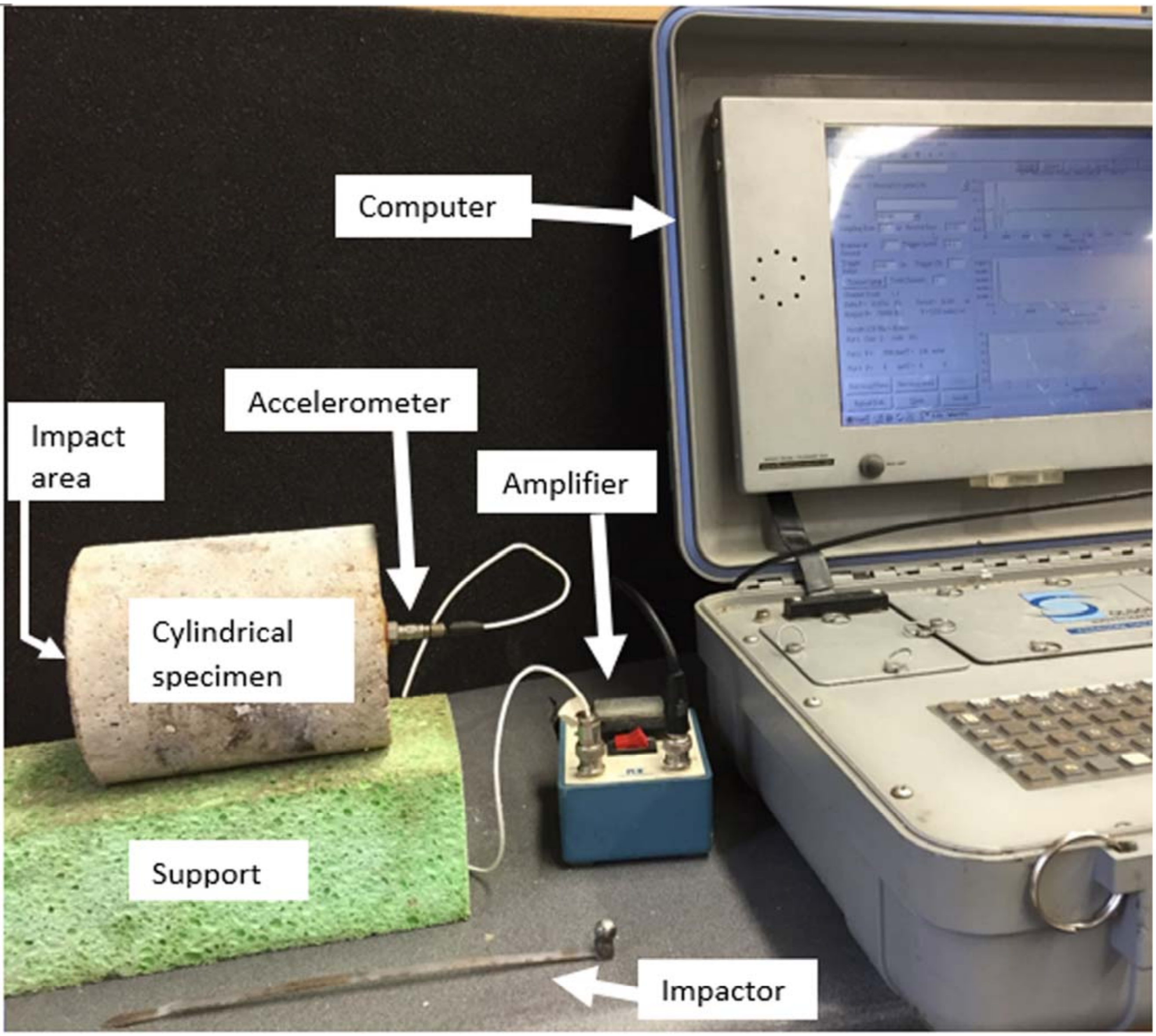
Computer
Accelerometer
Impact
area
Amplifier
Cylindrical
specimen
Support
Impactor

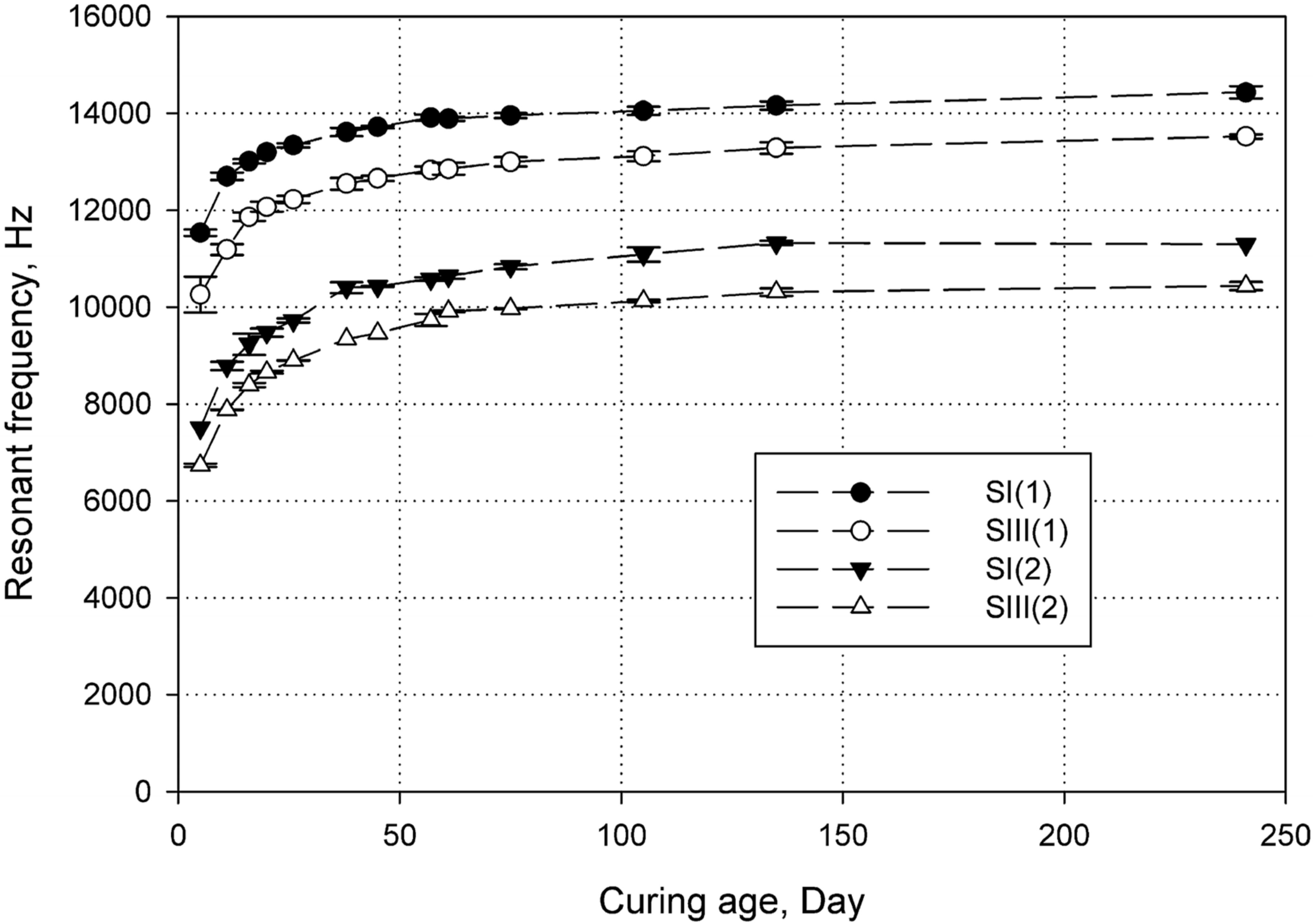

16000
14000
12000
10000
8000
6000
4000
2000
0
Resonant frequency, Hz
0
50
100
150
200
250
Curing age, Day
SI(1)
SIII(1)
SI(2)
SIII(2)

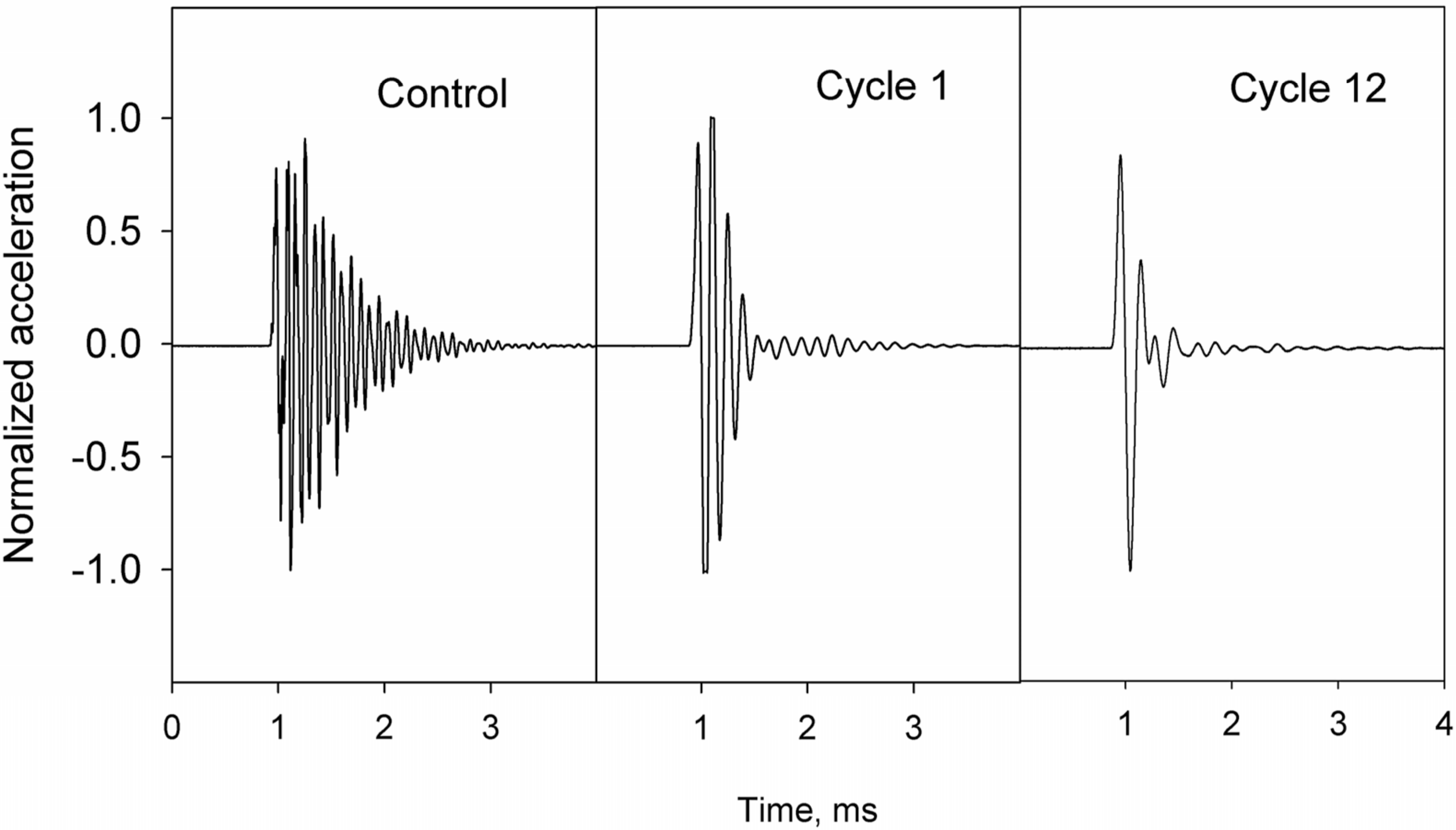
Control
Cycle 1
Cycle 12
Normalized acceleration
1.0
0.5
0.0
-0.5
-1.0
0
1
2
3
1
2
3
1
2
3
4
Time, ms

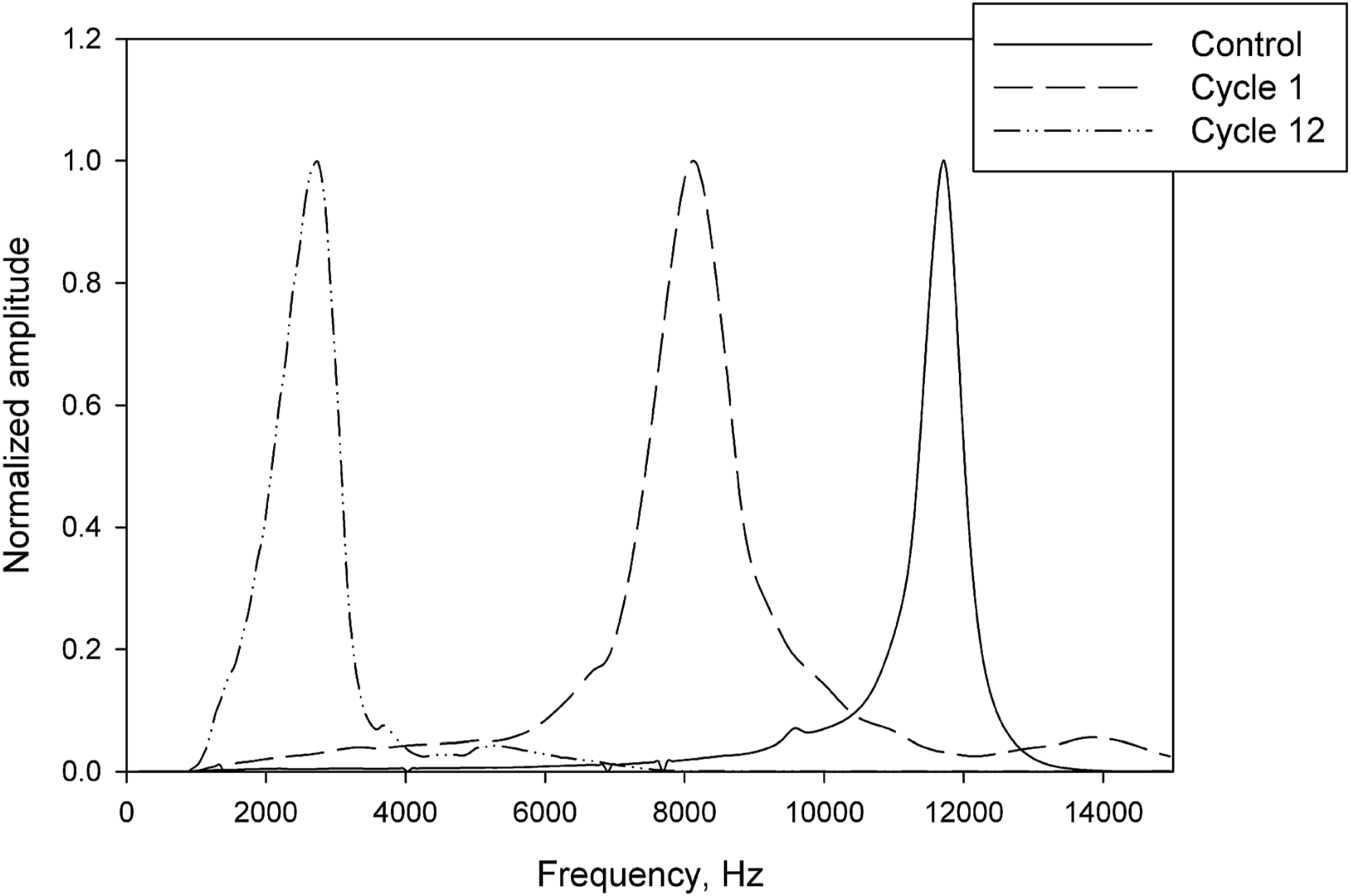
Control
Cycle 1
Cycle 12
1.2
1.0
0.8
0.6
0.4
0.2
0.0
Normalized amplitude
0
2000
4000
6000
8000
10000
12000
14000
Frequency, Hz

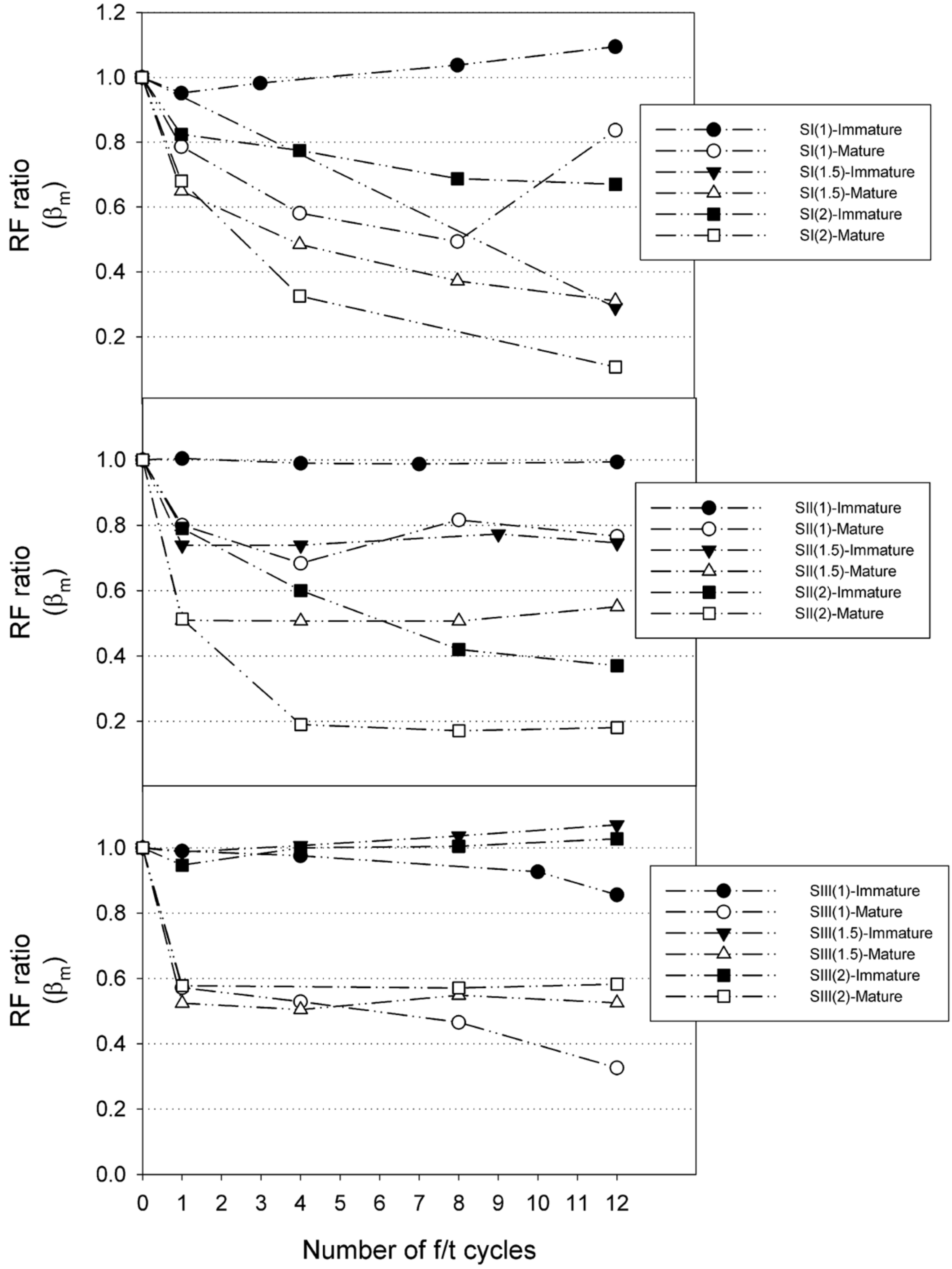

SI(1)-Immature
SI(1)-Mature
SI(1.5)-Immature
SI(1.5)-Mature
SI(2)-Immature
SI(2)-Mature
SII(1)-Immature
SII(1)-Mature
SII(1.5)-Immature
SII(1.5)-Mature
SII(2)-Immature
SII(2)-Mature
SIII(1)-Immature
SIII(1)-Mature
SIII(1.5)-Immature
SIII(1.5)-Mature
SIII(2)-Immature
SIII(2)-Mature
RF ratio (β_m)
Number of f/t cycles

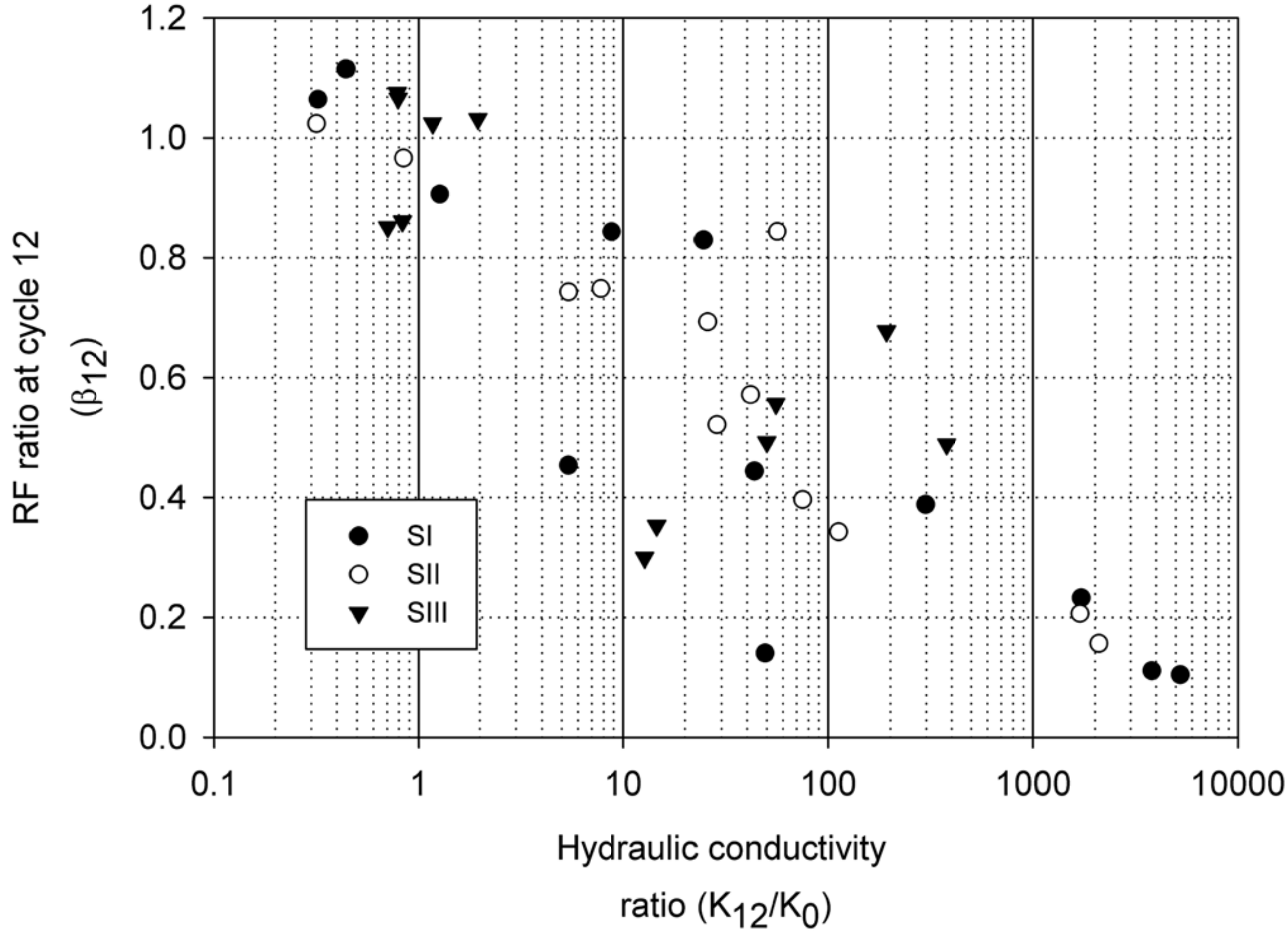
RF ratio at cycle 12 (β12)
1.2
1.0
0.8
0.6
0.4
0.2
0.0
0.1
1
10
100
1000
10000
SI
SII
SIII
Hydraulic conductivity ratio (K12/K0)

(A)

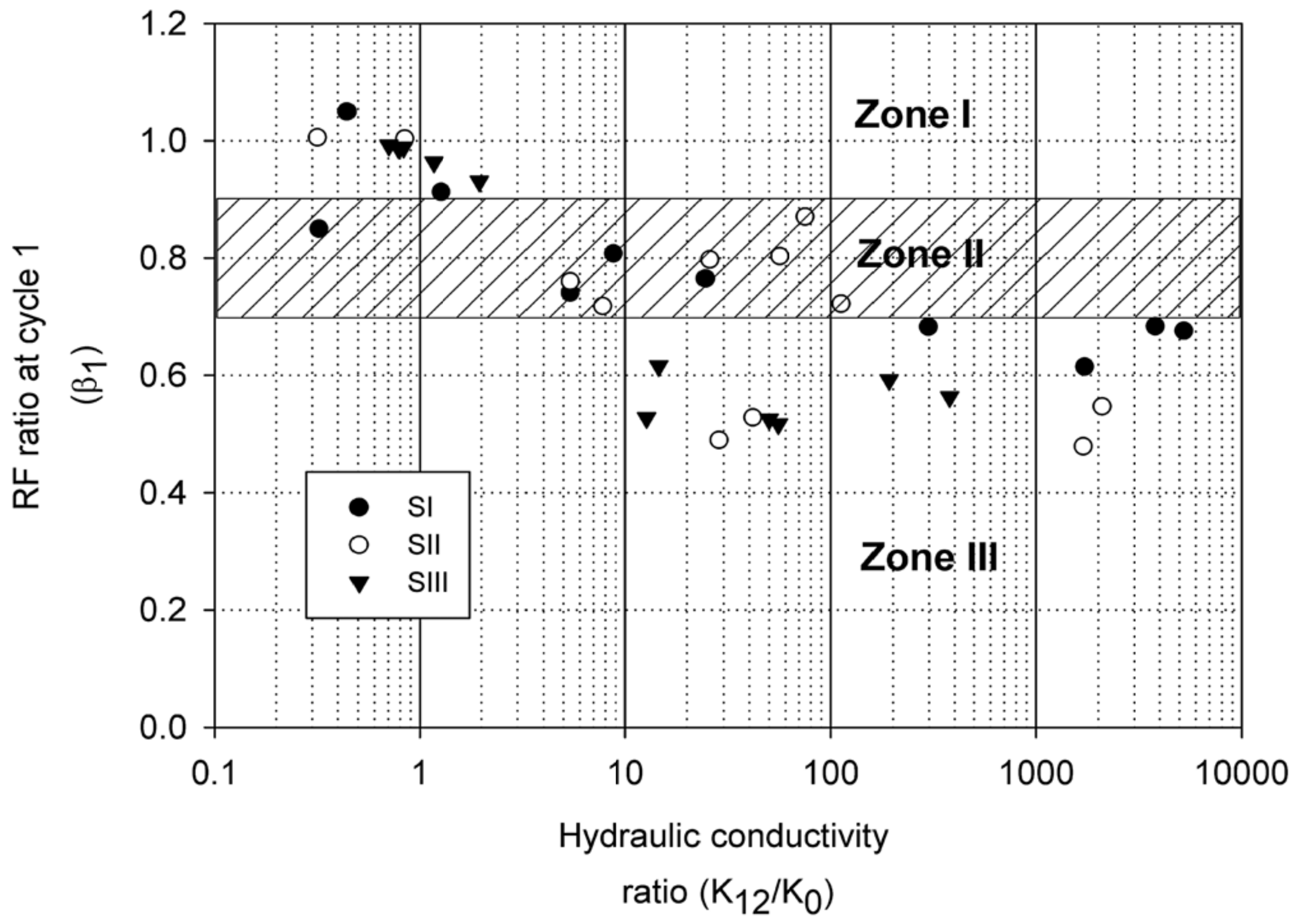
RF ratio at cycle 1 (β1)
1.2
1.0
0.8
0.6
0.4
0.2
0.0
0.1
1
10
100
1000
10000
Zone I
Zone II
Zone III
SI
SII
SIII
Hydraulic conductivity ratio (K12/K0)

(B)

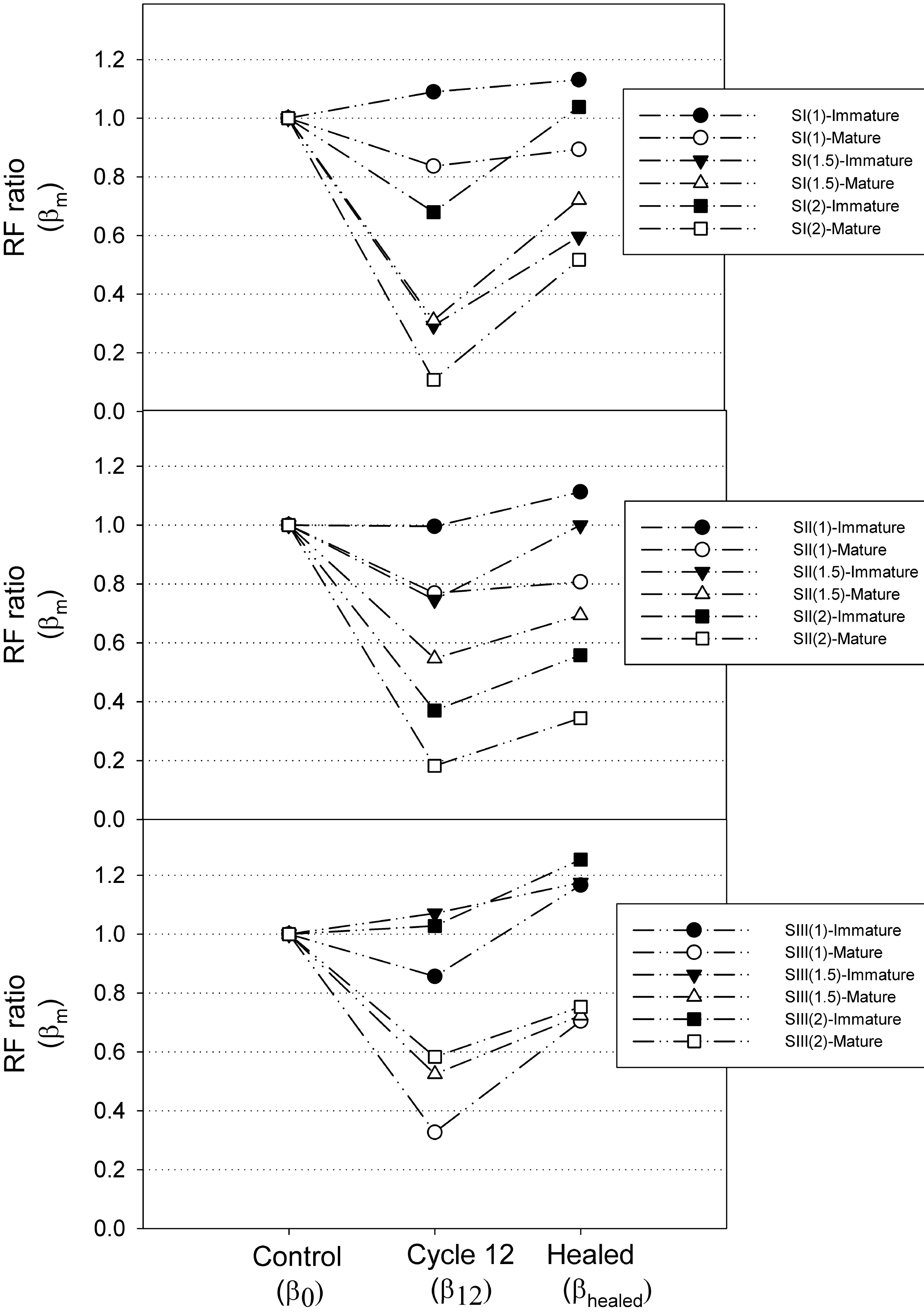

RF ratio (β_m)
1.2
1.0
0.8
0.6
0.4
0.2
0.0
SI(1)-Immature
SI(1)-Mature
SI(1.5)-Immature
SI(1.5)-Mature
SI(2)-Immature
SI(2)-Mature
SII(1)-Immature
SII(1)-Mature
SII(1.5)-Immature
SII(1.5)-Mature
SII(2)-Immature
SII(2)-Mature
SIII(1)-Immature
SIII(1)-Mature
SIII(1.5)-Immature
SIII(1.5)-Mature
SIII(2)-Immature
SIII(2)-Mature
Control (β_0)
Cycle 12 (β_{12})
Healed (β_{healed})

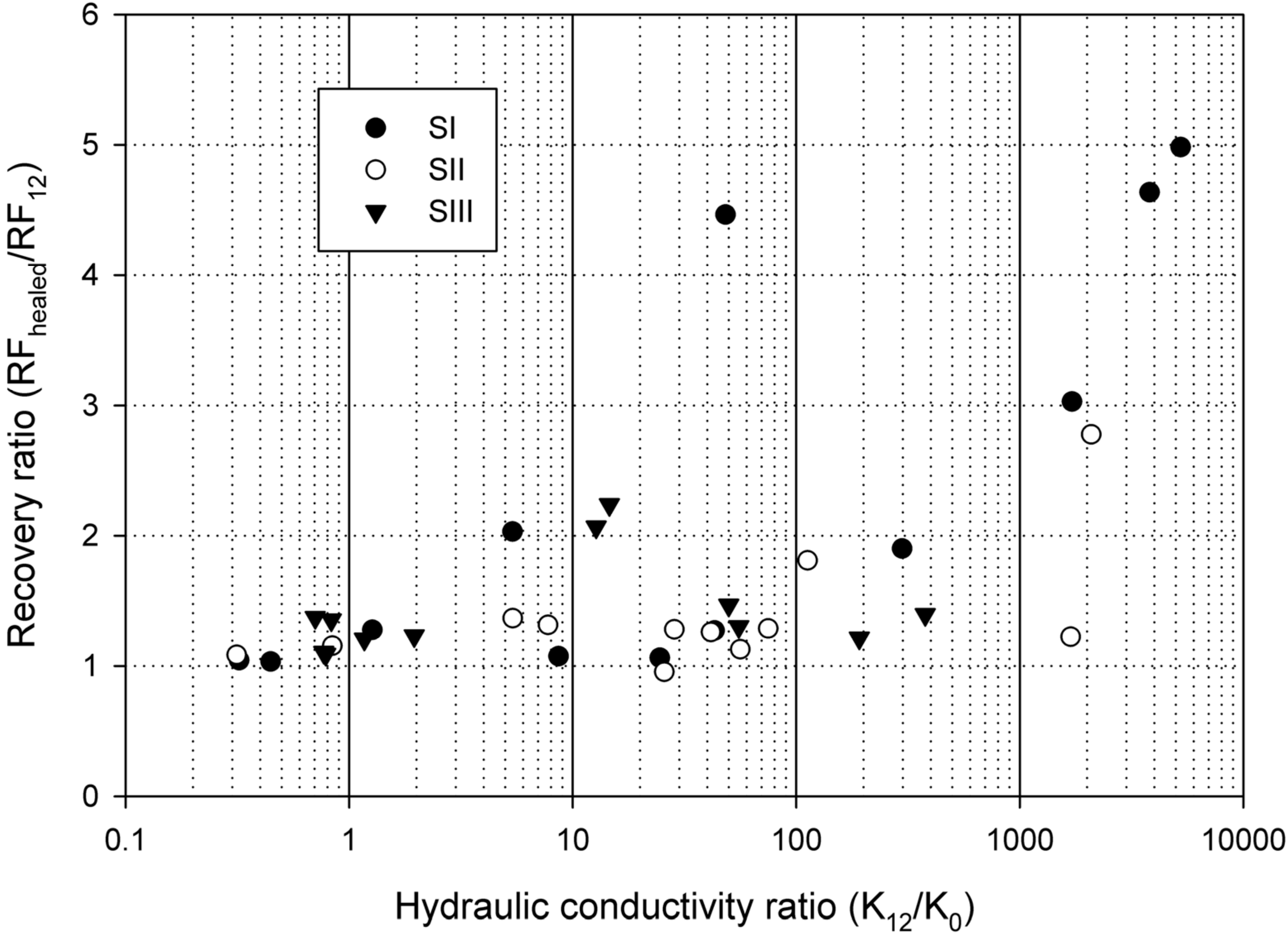

SI
SII
SIII
Recovery ratio (RF_{healed}/RF_{12})
Hydraulic conductivity ratio (K_{12}/K_0)
0
1
2
3
4
5
6
0.1
1
10
100
1000
10000